Virtual Thermal Ablation in the Head and Neck using Comsol MultiPhysics

Umit Topaloglu[1], Yulong Yan[2], Petr Novak[2], Paul Spring[3], James Suen[3] and Gal Shafirstein[3]*

[1] Department of Information Technology, University of Arkansas for Medical Sciences, USA
[2]Department of Radiation Oncology, University of Arkansas for Medical Sciences, USA.,
[3]Department of Otolaryngology, University of Arkansas for Medical Sciences, USA.,

* Corresponding author: G. Shafirstein, University of Arkansas for Medical Sciences, 501 Jack Stephens Drive, Little Rock, Arkansas 72205, shafirsteingal@uams.edu

Abstract: Thermal ablation in the head and neck requires accurate thermal dose delivery to target tissue while protecting the structure and function of nearby tissue and organs. In this study, we present a method that allows importing radiological images to Comsol modeling environment, in order to model accurately the expected pathological outcomes prior to thermal ablation treatment. As proof of concept, Computed Tomography (CT) scans of a human head were used as source images. Matlab was used to read Dicom™ images and to create intensity matrices. A non-linear median filtering was applied to reduce the noise without losing the object structure. After filtering an unsupervised k-means clustering was applied. The number of clusters was chosen to be k=4 to reflect 4 tissue types: bone, brain, connective tissue, and sinus. Object boundaries were identified with an edge-detection filter. Contours for each segmented object were located and converted into solid geometries that were imported to the Comsol 3.2. Thermal ablation of a virtual tumor was preformed for a conductive interstitial thermal therapy (CITT) device. The temperature fields were superimposed on the CT image. Importing images of anatomical structures into Comsol allows for a reliable model of heat distribution during thermal ablation of targeted tissue in head and neck that can be used for treatment planning, in the future.

Keywords: Thermal ablation, conductive interstitial thermal therapy (CITT), Computed Tomography (CT), DICOM, finite elements, Comsol.

1. Introduction

Thermal ablation techniques, such as radiofrequency ablation, laser ablation, cryotherapy, and focused ultrasound with MRI guidance, have shown promising results by destroying cancer cells via thermal energy delivery to target tissue. [1-8 9-17 18-24 25,26] A common denominator among all these techniques is that the generated heat is dissipated mainly by conduction to induce irreversible thermal damage by coagulation necrosis. Heat dissipation in conductive thermal ablation can be modeled using well-understood heat transfer principles.[27-29] We have recently demonstrated that conductive thermal ablation can be accurately model, using the Comsol, to predict the pathological outcomes of the thermal therapy.[30,31] In these works we presented a new thermal ablation device that is based on conductive interstitial thermal therapy or CITT. The CITT device is made from a power supply and customized metal probe. Heat is delivered to the tissue with an electrically heated ceramic covered metallic sphere placed at the end of the CITT probe that includes deployable pins, which can be retracted for insertion and removal of the CITT probe. The deployable metal pins enhanced heat transfer into the surrounding tissue. The pins differentiate the CITT device from the endometrial balloon ablation device that also induces thermal ablation by conduction.[27,28,32-34] The pins increase the effective surface area of the CITT probe. In addition, the rate of heat transfer to the tissue is increased since the thermal diffusivity of the metal pins is one order of magnitude larger than that of soft tissues. [35,36] The predictability and control of the CITT device was demonstrated by comparing calculated with observed thermal ablation depths demarcated with viability staining in fresh tissue resected from the treated region in breast tissue of live female pigs (swine model) and in a VX2 carcinoma model in live rabbits.[30,31] However, to translate these studies to

clinical settings more accurate simulation are required. To that end, we developed a method to import Computed Tomography (CT) scans into the Comsol environment, where virtual thermal ablation can be modeled as if the CITT probe is placed within a tissue cavity. As a proof of concept CT scans of a human head were used as source images. The image processing toolbox of Matlab was used to read Digital Imaging and Communications in Medicine (Dicom™) images and create intensity matrices. Contrast adjustments were performed for registration purposes. A non-linear median filtering was applied to reduce the noise without losing the object structure. After filtering an unsupervised k-means clustering was applied. The number of clusters was chosen to be k=4 to reflect 4 tissue types: bone, brain, connective tissue, and sinus. Object boundaries were identified with an edge-detection filter. Contours for each segmented object were located and converted into solid geometries that were imported to the Comsol 3.2. The temperature distribution during ablation was modeled with Comsol 3.2b and presented within the CT scans. Herein we present the method used to create the Comsol virtual ablation simulations. Whilst CT scans were used in this work, any DICOM™ images (e.g. from magnetic resonance imaging (MRI) or digital mammography) can be used to perform virtual ablation in the Comsol environment.

2. Theory and Governing Equations

The temperature distribution is calculated by solving the long-established equation for heat transfer by conduction and convection in perfused tissues (also so called the bioheat equation of Pennes) given by:[37-39]

$$\rho C(T)\frac{\partial T}{\partial t} - \nabla \cdot (k \nabla T) = Q - \rho C(T) \cdot \upsilon(T) \cdot (T_{art} - T) \quad \text{(Eq. 1)}$$

T is the temperature as a function of time (t); k is the thermal conductivity (W/m/°C); ρ is the density (kg/m^3); Q represents internal heat sources (W/m^3) and is set to zero because metabolic contributions are ignored in modeling conductive heating; [27,28,40] and υ(T) is the perfusion rate (m_b^3/m^3/sec; cubic meter of blood m_b in cubic meter of perfused tissue "m") as function of temperature, T.[27,41] It is assumed that the perfusion will cease when the temperature exceeds critical value (60 ºC).[42] $C(T)$ is the specific heat capacity (J/kg/°C) as a function of temperature (T) and includes the latent heat L (J/kg) for evaporation of the relative water content, in the tissue, at T=100°C. In this analysis we assumed that the liquid-to-gas transition occurs over 1°C, ΔT=1°C.

$$C(T) = C + \mathrm{L} \cdot \frac{\exp(-(\mathrm{T}-100)^2 / \Delta T^2)}{\sqrt{\Delta T^2 \pi}} \quad \text{(Eq. 1b)}$$

Following the phase transition, the specific heat returns to its original value. This method has been used previously in modeling laser heating of tissue, was validated in animal models, and agreed with clinical data. [30,31,41,43,44] Solving equation 1 provides the temperature as a function of space and time, $T(x, y, z, t)$. For initial conditions, the core tissue temperature (at time $t = 0$) was assumed to be 37 °C, and tissue external surface temperature was set at 26°C. Heating is simulated by changing the boundary condition (T(t)) at the outer boundary of the heating element coil at the point we measure and control the temperature, as detailed in Shafirstein Hennings et al. 2007 and Shafirstein Novak et al. 2007. [30,31]

The right side of equation 1 includes heat transfer via blood flow, where T_{art} is the arterial blood temperature, 37 °C. The boundary condition on external tissue surfaces exposed to natural convection by air is given by equation 2:

$$-k\nabla T = h_s (T - T_{amb}) \quad \text{(Eq. 2)}$$

where T_{amb} = 26 °C (the ambient temperature). The thermophysical parameters of the tissues were taken from Valvano 1995.[45] The effect of blood perfusion, included in the heat balance through υ(T), was assumed as 0.018 $m_b^3/m^3/s$ (mass of blood, m_b, per cubic meter per second).[30,31]

3. Numerical model

As proof of concept a Computed Tomography (CT) slide of a head region was used in this study. The modeling process, detailed in the appendix, included 5 steps; Image segmentation, filtering, creating contour to import to Finite Element (FE) software, and creating mesh.

a) Image Segmentation

Segmentation is a partition process of an image into subsamples to make it more meaningful and easy to process. The pixels are clustered based on some characteristic such as color, intensity, or texture.
K-means is the approach of choice in this work. In some applications, k-means groups given data into predefined (k) number of sub-regions by minimizing the Euclidean distance metric.[46] In our case, pixel intensity values are the values we cluster based on and k is predefined as 4 to reflect 4 tissue types: bone, brain, connective tissue, and sinus. It starts by partitioning the input points into 4 initial sets. It then calculates centroid of each set. It constructs a new partition by associating each point with the closest centroid. Then the centroids are recalculated for the new clusters until convergence.

Matlab Image processing toolbox for image import and segmentation processes were utilized. A CT slide in DICOM™ format was imported with "*dicomread*" function of image processing toolbox and intensity matrices were created (figure 1).

Figure 1 Imported CT scan into Matlab™.

Then K-means was applied to the imported image. It identified aforementioned 4 regions (figure 2).

Figure 2 Segmentation of the CT image identified brain, bone, sinus and connective tissue.

b) Filtering

Second step after segmentation is to identify object boundaries so that contours can be created. We have applied a gradient edge-detection filter. Since segmentation is already clustered regions based on intensity, edge detection became a non-trivial task. Contours for each segmented object were located (Figure 3).

Figure 3 Edge detection provides object boundaries.

c) Importing images to Comsol

In order to import to Comsol, geometries has to be converted into Comsol geometries. For that purpose inbuilt Comsol functions in Matlab utilized. First "*flim2curve"* has created a contour from the filtered image. "*geomcoerce"* then applied to the contour to create coerce geometry. Once coerce geometry created the CT image was imported into Comsol. Thereafter the CITT geometry was imported into the Comsol model and placed at the region where the

ablation was planned to be performed (see figure 4 below).

d) Mesh

Mesh quality and element size are the important factors for running FE analysis. Higher number of elements may result of running the model in excessive amount of time. These two entities depend on the preprocessing quality such as segmentation and filtering. Any existing overlay or cross may cause higher number of elements in mesh. After importing coerce geometry, mesh was initialized (Figure 4) using 1.3 growth rate and 0.3 curvature ("normal mesh" in Comsol).

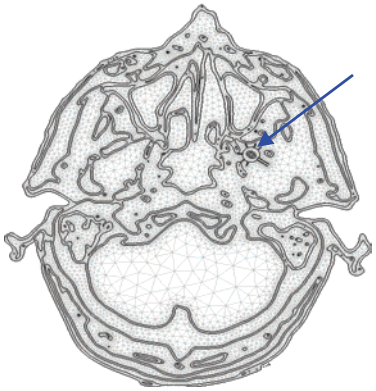

Figure 4. Mesh was applied to imported geometry. The blue arrow points at the CITT device.

Thermal ablation was modeled by increasing the temperature at a rate of 0.5 C/sec, at the center of the CITT probe to mimic thermal ablation therapy of CITT.[30,31] Ablation was simulated at maximum temperatures of 100, 130 and 150 C for 15 minutes.

4. Results and Discussion

The temperature distribution within the CT image was calculated for CITT ablation at maximum probe temperatures of 100, 130 and 150 °C at 15 minutes ablation time (figures 5 a-c). It is evident that at maximum probe temperature of 130 ^{o}C the ablation region is confine to the CITT probe, where the thermal damage will occur within the circumference defined by the CITT pins, which in this case are deployed to 3 mm away from the probe surface. In clinical settings the CITT can be placed under MRI guidance and the ablated region can be defined by the pins deployment.

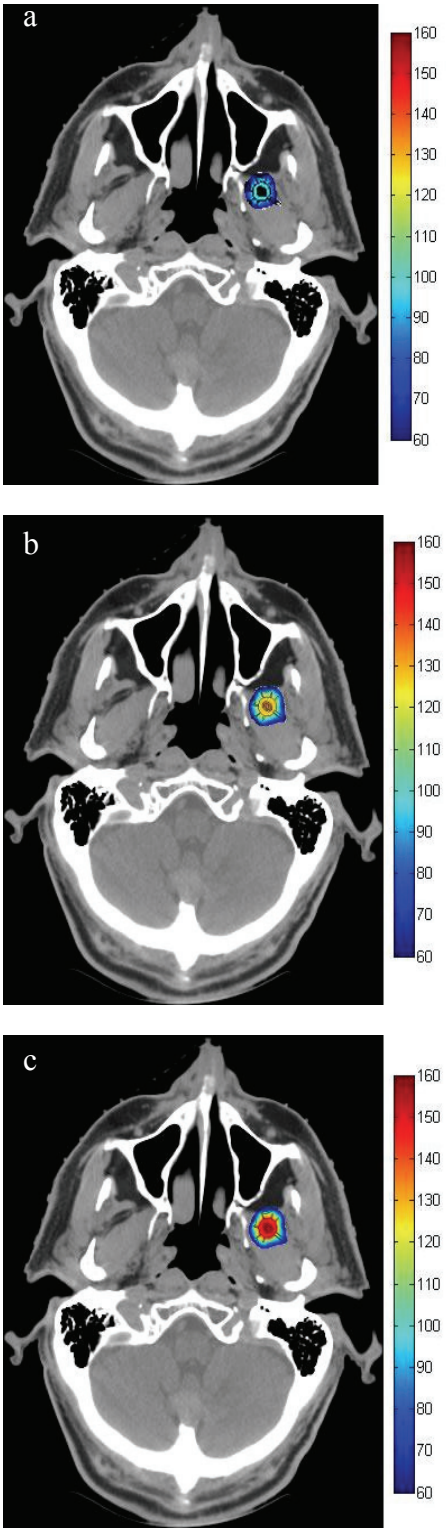

Figure 5. The calculated temperature distribution after 15 minutes CITT ablation at maximum probe temperature of 100 ^{o}C (a), 130 ^{o}C (b) and 150 ^{o}C (c).

Although the cooling and heating times affect the deposited thermal does, during high temperature CITT ablation the maximum temperature is the key parameter that dictates the size of the ablated region, as we demonstrated previously, in animal studies.[30,31]

The use of 2D slices limits the application of the current technique for actual treatment planning in clinical settings. Work is underway to use a series of 2D DICOM images to generate 3D geometries to simulate thermal ablation within the human body for accurate and reliable thermal ablation.

5. Conclusions

The segmentation method using k-means and edge detection was found to be reliable for differentiating tissue types in the head and neck. Solid objects were readily imported into the Comsol and meshed with a resolution better than 3 mm. Thermal ablation of a virtual tumor was preformed for a conductive interstitial thermal therapy (CITT) device. Modeling the heat transfer within anatomical structures enables us to determine the optimal parameters that will be required for a safe and effective thermal ablation therapy.

6. References

1 C. McCann and M. D. Sherar, Phys Med Biol 51, 3835-50 (2006).
2 C. McCann and M. D. Sherar, Phys Med Biol 51, 3851-63 (2006).
3 S. N. Goldberg, G. S. Gazelle, C. C. Compton, P. R. Mueller, and K. K. Tanabe, Cancer 88, 2452-63 (2000).
4 S. N. Goldberg, G. S. Gazelle, L. Solbiati, W. J. Rittman, and P. R. Mueller, Acad Radiol 3, 636-44 (1996).
5 T. Boehm, A. Malich, S. N. Goldberg, J. R. Reichenbach, I. Hilger, P. Hauff, M. Reinhardt, M. Fleck, and W. A. Kaiser, Radiology 222, 805-13 (2002).
6 T. Boehm, A. Malich, J. R. Reichenbach, M. Fleck, and W. A. Kaiser, Invest Radiol 36, 480-6 (2001).
7 F. Izzo, R. Thomas, P. Delrio, M. Rinaldo, P. Vallone, A. DeChiara, G. Botti, G. D'Aiuto, P. Cortino, and S. A. Curley, Cancer 92, 2036-44 (2001).
8 S. S. Jeffrey, R. L. Birdwell, D. M. Ikeda, B. L. Daniel, K. W. Nowels, F. M. Dirbas, and S. M. Griffey, Arch Surg 134, 1064-8 (1999).
9 D. W. Arthur, D. Koo, R. D. Zwicker, S. Tong, H. D. Bear, B. J. Kaplan, B. D. Kavanagh, L. A. Warwicke, D. Holdford, C. Amir, K. J. Archer, and R. K. Schmidt-Ullrich, Int J Radiat Oncol Biol Phys 56, 681-9 (2003).
10 M. Keisch, F. Vicini, R. R. Kuske, M. Hebert, J. White, C. Quiet, D. Arthur, T. Scroggins, and O. Streeter, Int J Radiat Oncol Biol Phys 55, 289-93 (2003).
11 W. P. Hogle, A. E. Quinn, and D. E. Heron, Clin J Oncol Nurs 7, 324-8 (2003).
12 T. A. King, J. S. Bolton, R. R. Kuske, G. M. Fuhrman, T. G. Scroggins, and X. Z. Jiang, Am J Surg 180, 299-304 (2000).
13 J. R. White and J. F. Wilson, Semin Surg Oncol 13, 190-5 (1997).
14 A. B. Akimov, V. E. Seregin, K. V. Rusanov, E. G. Tyurina, T. A. Glushko, V. P. Nevzorov, O. F. Nevzorova, and E. V. Akimova, Lasers Surg Med 22, 257-67 (1998).
15 A. M. Minhaj, F. Mann, P. J. Milne, D. B. Denham, N. Salas, Jr., I. Nose, K. Damgaard-Iversen, J. M. Parel, and D. S. Robinson, Phys Med Biol 47, 2987-99 (2002).
16 P. J. Milne, J. M. Parel, F. Manns, D. B. Denham, X. Gonzalez-Cirre, and D. S. Robinson, Lasers Surg Med 26, 67-75 (2000).
17 T. J. Vogl, M. G. Mack, A. Roggan, R. Straub, K. C. Eichler, P. K. Muller, V. Knappe, and R. Felix, Radiology 209, 381-5 (1998).
18 C. R. Hill and G. R. ter Haar, British Journal of Radiology 68, 1296-1303 (1995).
19 P. M. Harari, K. H. Hynynen, R. B. Roemer, D. P. Anhalt, D. S. Shimm, B. Stea, and J. R. Cassady, International Journal of Radiation Oncology, Biology, Physics 21, 831-40 (1991).
20 Gianfelice DC, Mallovche H, and Lepanto L, in MR-guided focused ultrasound ablation of primary breast neoplasms: works in progress. [Abstract]. Chicago. Oak Brook (IL), 1999 (RSNA).
21 S. E. Singletary, Semin Surg Oncol 20, 246-50 (2001).
22 C. J. Diederich, Int J Hyperthermia 21, 745-53 (2005).
23 C. J. Diederich and K. Hynynen, Ultrasound Med Biol 25, 871-87 (1999).
24 C. J. Diederich, W. H. Nau, A. B. Ross, P. D. Tyreus, K. Butts, V. Rieke, and G. Sommer, Int J Hyperthermia 20, 739-56 (2004).

25 Rabin Y, Julian TB, and Olson P, Proceedings SPIE (International Society of Optical Engineering) 3590, 465-471 (1999).
26 E. D. Staren, M. S. Sabel, L. M. Gianakakis, G. A. Wiener, V. M. Hart, M. Gorski, K. Dowlatshahi, B. F. Corning, M. F. Haklin, and G. Koukoulis, Archives of Surgery 132, 28-33; discussion 34 (1997).
27 S. A. Baldwin, A. Pelman, and J. L. Bert, Ann Biomed Eng 29, 1009-18 (2001).
28 D. P. Orgill, M. G. Solari, M. S. Barlow, and N. E. O'Connor, J Burn Care Rehabil 19, 203-9 (1998).
29 E. Y. Ng and L. T. Chua, Burns 28, 27-34 (2002).
30 G. Shafirstein, L. Hennings, Y. Kaufmann, P. Novak, E. G. Moros, S. Ferguson, E. Siegel, S. V. Klimberg, M. Waner, and P. Spring, Technol Cancer Res Treat 6, 235-46 (2007).
31 G. Shafirstein, P. Novak, E. G. Moros, E. Siegel, L. Hennings, Y. Kaufmann, S. Ferguson, J. Myhill, M. Swaney, and P. Spring, Int J Hyperthermia 23, 477-92 (2007).
32 A. Singer, R. Almanza, A. Gutierrez, G. Haber, L. R. Bolduc, and R. Neuwirth, Obstet Gynecol 83, 732-4 (1994).
33 A. Gallinat, Contrib Gynecol Obstet 20, 137-44 (2000).
34 R. S. Neuwirth, A. A. Duran, A. Singer, R. MacDonald, and L. Bolduc, Obstet Gynecol 83, 792-6 (1994).
35 J. D. Bronzino, The biomedical engineering handbook (CRC Press: IEEE Press, Boca Raton, 1995).
36 J. P. Holman, Heat transfer, 6th ed. (McGraw-Hill Book Co., New York, 1986).
37 Optical-thermal response of laser-irradiated tissue; Vol., edited by A. J. Welch and M. J. C. v. Gemert (Plenum Press, New York, 1995).
38 E. H. Wissler, J Appl Physiol 85, 35-41 (1998).
39 H. H. Pennes, Journal of Applied Physiology 1, 93-122 (1948).
40 D. M. Reinders, S. A. Baldwin, and J. L. Bert, Journal of Biomechanical Engineering 125, 841-51 (2003).
41 G. Shafirstein, W. Baumler, M. Lapidoth, S. Ferguson, P. E. North, and M. Waner, Lasers Surg Med 34, 335-47 (2004).
42 J. Heisterkamp, R. van Hillegersberg, and I. J. JN, Lasers Surg Med 25, 257-62 (1999).
43 P. Babilas, G. Shafirstein, W. Baumler, J. Baier, M. Landthaler, R. M. Szeimies, and C. Abels, J Invest Dermatol 125, 343-52 (2005).
44 W. Baumler, H. Ulrich, A. Hartl, M. Landthaler, and G. Shafirstein, Br J Dermatol 155, 364-71 (2006).
45 J. W. Valvano, in Optical-thermal response of laser-irradiated tissue, edited by A. J. Welch and M. J. C. v. Gemert (Plenum Press, New York, 1995), p. 445-489.
46 R. Nagarajan, IEEE Trans Med Imaging 22, 882-9 (2003).

8. Acknowledgments

This work was supported, in part, by the National Cancer Institute NIH/NCI Grant No. 5R21 CA108678-01.

9. **Appendix**

```
clear all
clc
for i=1:97
if (i<10)
dummy=['hn_sample00' num2str(i) '.dcm'];
else
dummy=['hn_sample0' num2str(i) '.dcm'];
end
I = dicomread(dummy);

%filter removes some noise
medfilt=medfilt2(I);
k=4;
[mu{i},mask{i}]=kmeans(medfilt,k);

%edge detection filter
A= mask{i};
C= mask{i};

for t=2:size(A,1)-1
   for j=2:size(A,2)-1

       if (abs(A(t+1,j)-A(t-1,j))>0  ...
         || abs(A(t,j+1)-A(t,j-1))>0)
       C(t,j)=1;
        j=j+1;
      else
        C(t,j)=0;
      end
   end
end

%% convert to Comsol objects

 %contour
```

```
    eval(['contour' num2str(i) '=
flim2curve(flipdim(C,1),{[],[.5 .5]});'])

 %solid
   eval(['Solid' num2str(i) '=
geomcoerce("solid",contour' num2str(i) ');'])
end
```